Available online at www.sciencedirect.com
ScienceDirect
Scripta Materialia 64 (2011) 205–208
Scripta MATERIALIA
www.elsevier.com/locate/scriptamat

Novel magnetodielectric nanomaterials with matching permeability and permittivity for the very-high-frequency applications

Atul Thakur,[a] Preeti Thakur[b] and Jen-Hwa Hsu[a,*]

[a]*Department of Physics, National Taiwan University, Taipei 106, Taiwan*
[b]*Physics Department, Himachal Pradesh University, Shimla 171005, India*

Received 18 August 2010; revised 28 September 2010; accepted 29 September 2010
Available online 14 October 2010

Nanoferrites with a composition of $Ni_{0.35}Zn_{0.35}Co_{0.2}Mn_{0.05}Cu_{0.05}Fe_{1.98}O_4$ were synthesized by a co-precipitation method. The material obtained after sintering at 900 °C shows almost matching permeability and permittivity values of close to 6 with low values for magnetic loss tangent (~0.03) and dielectric loss tangent (~0.008) in the range 10–200 MHz. Together with a refractive index of about six and a reduced impedance of around one, this material could be employed for loading of miniaturized antennas in the VHF band.

Keywords: Precipitation; Nanocomposite; Ceramics; Sintering; Dielectric

Conventional VHF antennas have large physical dimensions and existing approaches to reduce their size degrade their performance [1]. Reducing the physical dimensions of such antennas without affecting their electric performance remains a challenging task. There are a few approaches for patch antenna miniaturization. The first approach is to use capacitive or inductive loadings. The major drawback of this method is entrapment of a large amount of electromagnetic energy within the near-field region. In addition, due to the strong resonance and increased losses, antenna efficiency is expected to be low [2]. The second approach is to use dielectric materials for loading. However, dielectrically loaded antennas are prone to surface wave excitations [3]. Using only high-permittivity or dielectric materials for device miniaturization causes serious problems, such as impedance mismatch and increased mutual coupling between the components. The third approach is to utilize magnetodielectric materials for loading [4]. This technique is quite useful as permeability also contributes to miniaturization [5]. Moreover, a smaller value for permittivity is required to achieve the same miniaturization factors as compared to pure dielectric loading [6].

Magnetodielectric materials with a high refractive index and impedance matched to the free space have many potential electromagnetic applications. However, such materials are not found in nature. A chessboard structure has been proposed by Yu et al. [7] to achieve equal values of relative permeability and permittivity. Kong et al. [8] suggested composite materials based on polycrystalline ferrite and epoxy. Petrov et al. [9] proposed ferrite–ferroelectric-based composite for antenna miniaturization. However, these studies based on fully sintered ceramics are applicable for antenna miniaturization only below 100 MHz [1,9–10].

The present study aims to investigate materials with almost equal values of permeability and permittivity for antenna design in the radiofrequency range. It is well known that polycrystalline ferrites generally have higher permeability than permittivity, while metal alloys have higher permittivity than permeability because of their high conductivity. Cobalt is useful for shifting the relaxation due to its high magnetocrystalline anisotropy, and copper is a good sintering aid [8,10]. Deficiency in iron and addition of manganese are helpful in suppressing the formation of Fe^{2+} ions and maintaining low dielectric loss tangents. Therefore, in the present paper, we propose porous and spinel nanoferrites with a composition of $Ni_{0.35}Zn_{0.35}Co_{0.2}Mn_{0.05}Cu_{0.05}Fe_{1.98}O_4$, which have almost equal values of permeability and permittivity, as low-loss magnetodielectric materials enabling antenna miniaturization in the radiofrequency range.

* Corresponding author. Tel.: +886 2 33665162; fax: +886 233665892; e-mail: jhhsu@phys.ntu.edu.tw

1359-6462/$ - see front matter © 2010 Acta Materialia Inc. Published by Elsevier Ltd. All rights reserved.
doi:10.1016/j.scriptamat.2010.09.045

Nanoferrites of composition $Ni_{0.35}Zn_{0.35}Co_{0.2}Mn_{0.05}Cu_{0.05}Fe_{1.98}O_4$ were prepared by a co-precipitation method [11]. High-purity chemicals used were nickel chloride, zinc chloride, cobalt chloride, manganese chloride, copper chloride, iron(III) chloride and sodium hydroxide. The chemicals with accurate stoichiometric proportions were prepared in double-distilled water and mixed quickly into a boiling solution of NaOH (0.40 mol l^{-1}) under vigorous stirring. Mixing is very important as otherwise segregation of phases can take place. After co-precipitation, the pH was set at 11.5 by adding NaOH solution dropwise. Reaction was continued for 30 min at a temperature of 90 °C under vigorous stirring. The suspension was cooled to ambient temperature and then reduced to ~400 ml by removal of the supernatant. The suspension was then centrifuged at 5000 rpm for 15 min, and the resulting precipitate washed carefully with distilled water to remove any impurities. The residue was dried in an electrical oven overnight. The ferrite powders were pre-sintered at a temperature of 800 °C in air for 3 h at heating and cooling rates of 200 °C h^{-1}, mixed with 3% polyvinyl alcohol solution as binder and then compacted into a toroidal shape under a pressure of 32 MPa. These toroidal samples were finally sintered in air at a temperature of 900 °C (sample I) and 950 °C (sample II) for another 3 h, each at a heating and cooling rate of 200 °C h^{-1}.

X-ray diffraction (XRD) measurements were performed on a Philips PW 1729 diffractometer using Cu Kα radiation. Transmission electron microscopy (TEM) images were obtained with a JEOL JEM-100CX and scanning electron microscopy (SEM) images were recorded on a Hitachi S-3200 N. Density measurements were undertaken on a Micromeritics Accupyc II 1340 Pycnometer. Complex permeability and permittivity were measured using an impedance analyzer (HP4291B).

XRD patterns of the sample pre-sintered at 800 °C, and sintered at 900 and 950 °C are shown in Figure 1a–c, respectively. The patterns show all the characteristic peaks of a cubic spinel structure and confirm the phase formation, indicating the absence of other impurity or unreacted constituents. The XRD patterns exhibit broad peaks, indicating the ultrafine nature and small crystalline size of the particles. The broadening of the peaks is found to reduce with sharp intensities after sintering for sample I, indicating grain growth during the sintering process. Similar behaviour has been observed for sample II with relatively sharp and intense peaks. The average particle size D of the sample was estimated with the most prominent peak (3 1 1), by using the Debye–Scherer formula for Lorentzian peaks [12]. The value for D is about 22 nm for the sample before sintering, 32 nm for sample I and 44 nm for sample II after sintering. The lattice parameter was determined using Bragg's law [11]. The values are 0.8377 and 0.8389 nm for samples I and II, respectively, which are in close agreement with the literature data for Ni–Zn ferrites [13].

Figure 2a displays TEM image of the pre-sintered ferrite powder. The powder appears to be non-agglomerated and the particle size is found to be narrowly distributed. The nanoparticles are almost uniform, monodispersed and cubic in shape. The average particle size is about 25 nm, which is quite consistent with that of the

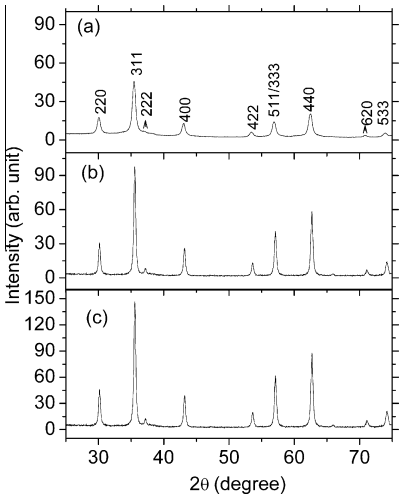

Figure 1. XRD patterns of ferrite sample (a) pre-sintered at 800 C, (b) sample I and (c) sample II.

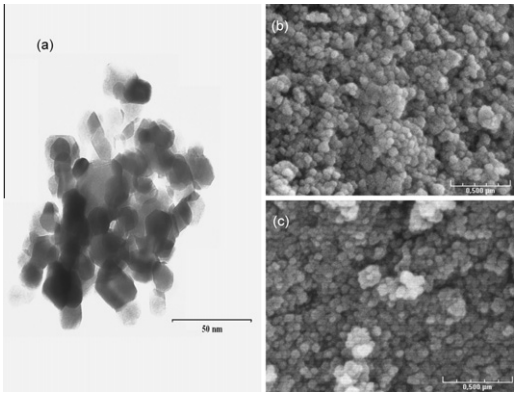

Figure 2. (a) TEM image of the ferrite powder pre-sintered at 800 °C; (b) SEM images of sample I and (c) sample II.

XRD results. Figure 2b and c display SEM images of the fractured surface of sample I and sample II, respectively. The sintering temperature has a great influence on the microstructure. It is observed that the average grain size of the sample increases with increasing sintering temperature. Consequently, the density (porosity) is found to increase (decrease). The porosity is found to be about 14% for sample I and 11% for sample II due to the grain growth during the sintering process. As a result of aggregation of a large number of crystallites due to pressing [14] and grain growth during sintering, the average grain size is found to be about 50 nm. The observed value is much lower than the critical limit for multidomain grains [15,16].

The frequency response of the complex permeability and permittivity spectra of sample I and sample II is plotted in Figure 3a and b, respectively. The complex permeability (μ^*) of sintered ferrite can be described as [17,18]:

$$\mu^* = \mu' - \mu'' = 1 + \chi_{sp} + \chi_{dw} \quad (1)$$

where μ' is the real part of permeability, μ'' is the imaginary part of permeability, χ_{sp} is the spin rotational susceptibility, and χ_{dw} is the domain wall susceptibility. The

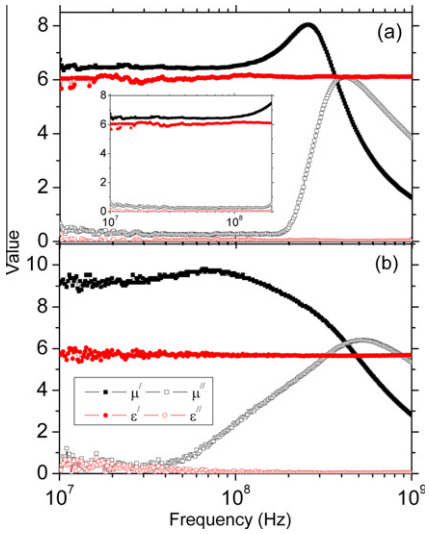

Figure 3. Complex permeability and permittivity spectra of (a) sample I and (b) sample II. Inset picture in (a) depicts the results between 10 and 200 MHz for sample I.

spin rotational component is of relaxation type and its dispersion is inversely proportional to the frequency. The domain wall component is of resonance type and depends on the square of frequency [19]. In the present study, the permeability spectra for both samples show a common feature. For sample I, μ' remains almost constant up to 200 MHz with a value of ~6.4, then increases to a maximum value of 8.2, beyond which μ' begins to decrease. The imaginary permeability μ'' remains very low with a value of ~0.22 at frequencies below 200 MHz, and then increases to a maximum. For sample II, μ' also attains a constant value of ~9.2 but only up to 40 MHz. After that, it shows a continuous increase until a maximum value of ~9.9 at 75 MHz, and then finally decreases. Since in the present study the average grain size is smaller than the critical size for multidomain grains, the contribution of χ_{dw} to μ^* can therefore be neglected and the observed low values of permeability may be linked to the spin rotational contributions only. For both samples, at around the frequency where μ' becomes half of the constant value, μ'' shows a broad peak due to relaxation. In general, the relaxation frequency f_r and the static permeability μ_s for spinel ferrite materials can be expressed by Snoek's law [20]:

$$(\mu_s - 1) f_r = C \tag{2}$$

where $C = \frac{2}{3}(\gamma . M_S)$ where γ is the gyromagnetic ratio and M_s is the saturation magnetization. Therefore, a larger static permeability leads to a lower relaxation frequency [21].

Sintering temperature has a great influence on magnetic properties. As the sintering temperature is increased, both real and imaginary parts of the complex permeability increase. An increase in the real part of the permeability by ~40% is seen as the sintering temperature increases from 900 to 950 °C. This increase in permeability may be due to grain growth and reduced porosity at the elevated sintering temperature. In porous materials, magnetic poles are created on the surface of grains/particles under the applied magnetic field. As a consequence, a demagnetizing field is produced, leading to a decrease in static permeability [10]. For sample II, the relaxation in the imaginary part is quite broad and started at a very low frequency of 40 MHz, indicating that nucleation at a sintering temperature of 950 °C occurs as a single event, leading to a nonuniform and discontinuous grain growth; whereas at a sintering temperature of 900 °C, the relaxation starts at a relatively higher frequency beyond 200 MHz (inset of Fig. 3a). The sharp relaxation peak and constant permeability value over a wide range of frequency for sample I may be attributed to slow nucleation at a sintering temperature of 900 °C, leading to uniform and homogenous grain growth. The relaxation behaviour of permeability spectra, i.e. the low value of μ' associated with the high value of relaxation frequency can be linked to the monodomain grains having rotational permeability and to the porous microstructure of the ferrite. The porous ferrites are regarded as composite materials with a high ferrite ratio [22]. Therefore, the porosity of 14% for sample I is a suitable value for antenna applications in the VHF range.

High-frequency permittivity of ferrite materials is mainly contributed by the atomic and electronic polarization. Fe^{2+} ions in ferrite materials always enhance the permittivity due to these ions having a larger polarization than Fe^{3+} ions. Fe^{3+} ions have a spherical symmetry of the charge electron cloud due to a stable *d*-shell configuration, whereas Fe^{2+} ions have an extra electron which disturbs the symmetry of the charge electron cloud [23]. Therefore, the presence of Fe^{2+} ions in the ferrite sample increases polarization and hence permittivity. However, high permittivity in the present study is undesirable because it is accompanied by high losses.

In the present study, the complex permittivity contributed by atomic and electronic polarization is almost independent of frequency over 10 MHz–1 GHz. Both the real and imaginary permittivity stays almost flat over the entire frequency range. However, as the sintering temperature is increased from 900 to 950 °C, a drop in the real part of the permittivity of ~7% is noticed. The dielectric properties of polycrystalline ferrite ceramics are additionally affected by microstructure, grain size, density (porosity) and impurities of the samples. The densification by sintering occurs in three steps as follows: bridge formation between the grain, granular arrangements and then grain growth [24]. The grain size effect on the permittivity is explained by the Maxwell–Wagner effect [23,25], which, in ferrites, arises due to the highly conducting grains separated by the layers of lower conductivity. These observations show that low dielectric constants are associated with stoichiometric ferrites. In addition, porosity has a strong influence on the permittivity of the ferrite materials. Closed pores will reduce the permittivity, whereas open pores may increase permittivity. Real and imaginary parts of permittivity for both samples show some frequency dependence in the lower-frequency range. This may be attributed to the electrical conduction of the sample due to their poor densification properties.

The refractive index ($n = \sqrt{\mu' \times \varepsilon'}$), reduced impedance ($Z/Z_0 = \sqrt{\mu'/\varepsilon'}$), dielectric and magnetic loss tangents for sample I are plotted in Figure 4. Sample I has

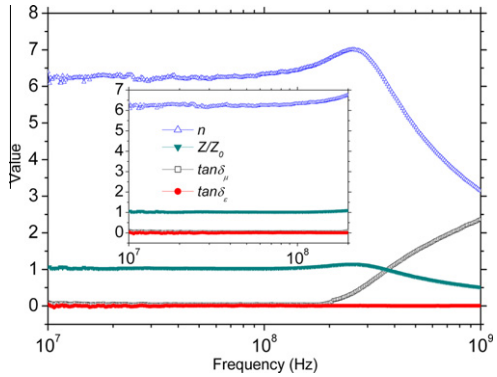

Figure 4. Refractive index, reduced impedance and loss tangents of sample I. Inset picture depicts the results between 10 and 200 MHz.

almost identical values for permeability and permittivity over 10–200 MHz, which results in a Z/Z_0 of close to 1 and an n of close to 6.3. This value of the refractive index is sufficient to reduce the size of antenna by a factor of ~6. Kong et al. [10] were successful in miniaturizing the antenna by a factor of 13–15 with unchanged electric dimension by using Li–Co ferrite. However, their frequency of interest was 10–30 MHz. In polycrystalline ferrite ceramics, dielectric loss tangent arises from the lag in polarization vis-à-vis applied electric field, whereas magnetic loss tangent results from the lag in magnetization vis-à-vis applied magnetic field. A single-phase ferrite structure free from impurities and imperfections and produced by a co-precipitation method resulted in low dielectric loss tangents in the present study. Moreover, the deficiency in iron and addition of manganese are helpful to suppress the formation of Fe^{2+} ions and maintain low dielectric loss tangents. The low permeability loss tangents are linked to the stoichiometric ferrites with homogeneous and uniform grains [26]. It is interesting to note that very low loss tangents ($\leqslant 10^{-2}$) are required to minimize losses in the antenna. In particular, a sufficiently low dielectric loss tangent is one of the critical requirements for antenna applications [27]. In this respect, sample I with a dielectric loss tangent of 0.008 may find practical application for miniaturization of antennas in the VHF bands. The miniaturization of antennas by the use of high dielectric materials with a small permeability results in low efficiency and a narrow bandwidth [28]. Magnetodielectric materials have no such problem. These materials can be used to miniaturize antenna by the same factor by using moderate and matching values of μ' and ε'.

In summary, magnetodielectric nanomaterials based on ferrite powders with composition $Ni_{0.35}Zn_{0.35}Co_{0.2}Mn_{0.05}Cu_{0.05}Fe_{1.98}O_4$ for antenna miniaturization were fabricated and characterized. In particular, sample I sintered at 900 °C is found to be useful with an average grain size of 50 nm and 14% porosity. The measured μ' and ε' both remain almost identical (~6), while the magnetic and dielectric loss tangents show values close to 0.03 and 0.008, respectively, in the frequency range from 10–200 MHz. These materials have been demonstrated to be suitable for the design of VHF antennas with reduced physical dimensions.

The authors would like to thank the National Science Council of Taiwan, for financially supporting this research under Contract No. NSC-96-2112-M-002-006-MY3 and the Ministry of Economic Affairs of Taiwan under Grant No. 99-EC-17-A-08-S1-006.

[1] J. Holopainen, J. Villanen, M. Kyro, C. Icheln; P. Vainikainen, IEEE International Workshop on Antenna Technology: Small Antenna and Novel Metamaterials, 6–8 March 2006, pp. 305–308.
[2] H. Liu, S. Ishikawa, A. An, S. Kurachi, T. Yoshimasu, Microwave Opt. Technol. Lett. 49 (2007) 2438.
[3] A. Hoorfar, A. Perrotta, IEEE Trans. Antennas Propag. 49 (2001) 838.
[4] K. Sarabandi, R. Azadegn, H. Mosallaei, J. Harvey, Antenna Miniaturization Techniques for Applications in Compact Wireless Transceivers, XXVIIth, General Assembly of URSI, Maastricht, The Netherlands, 2002.
[5] H. Mosallaei and K. Sarabandi, Periodic Meta-material Structures in Electromagnetics: Concept, Analysis, and Applications, IEEE AP-S International Symposium, San Antonio, TX, 2002.
[6] R.V. Petrov, A.S. Tatarenko, S. Pande, G. Srinivasan, J.V. Mantese, R. Azadegan, Elec. Lett. 44 (2008) 528.
[7] W. Yu, R. Mitra, D.H. Werner, Guided Wave Lett. 9 (1999) 496.
[8] L.B. Kong, Z.W. Li, G.Q. Lin, Y.B. Gan, IEEE Trans. Magn. 43 (2007) 6.
[9] R.V. Petrov, A.S. Tatarenko, G. Srinivasan, J.V. Mantese, Microwave Opt. Technol. Lett. 50 (2008) 3154.
[10] L.B. Kong, M.L.S. Teo, Z.W. Li, G.Q. Lin, Y.B. Gan, J. Alloy. Compd. 459 (2008) 576.
[11] P. Mathur, A. Thakur, M. Singh, J. Magn. Magn. Mater. 320 (2008) 1364.
[12] A. Thakur, P. Mathur, M. Singh, J. Phys. Chem. Solids 68 (2007) 378.
[13] P. Mathur, A. Thakur, M. Singh, G. Harris, Z. Phys. Chem. 222 (2008) 621.
[14] P. Priyadharsini, A. Pradeep, G. Chandrasekaran, J. Magn. Magn. Mater. 321 (2009) 1898.
[15] K. Kawano, M. Hachiya, Y. Iijima, N. Sato, Y. Mizuno, J. Magn. Magn. Mater. 321 (2009) 2488.
[16] P.J. van der Zaag, M.T. Johnson, A. Noordermeer, P.T. Por, M.Th. Rekveldt, J. Magn. Magn. Mater. 99 (1999) L1.
[17] H. Su, H. Zhang, X. Tang, Y. Jing, J. Appl. Phys. 103 (2008) 093903.
[18] H. Su, H. Zhang, X. Tang, Y. Jing, Z. Zhong, J. Alloy. Compd. 481 (2009) 841.
[19] T. Nakamura, J. Magn. Magn. Mater. 168 (1997) 285.
[20] J.-L. Snoek, Physica 14 (1948) 207.
[21] L.B. Kong, Z.W. Li, G.Q. Lin, Y.B. Gan, IEEE Trans. Magn. 44 (2008) 559.
[22] T. Tsutaoka, J. Appl. Phys. 93 (2003) 2789.
[23] A. Verma, D.C. Dube, J. Am. Ceram. Soc. 88 (2005) 519.
[24] R. Valenzuela, Magnetic Ceramics, Cambridge University Press, Cambridge, 1994, pp. 70.
[25] P.A. Miles, W.B. Westphal, A. von Hippel, Rev. Mod. Phys. 29 (1957) 279.
[26] W.D. Kingery, H.K. Bowen, D.R. Uhlmann, Introduction to Ceramics, 2nd ed., Wiley, New York, 1976, pp. 913–945.
[27] L.B. Kong, Z.W. Li, G.Q. Lin, Y.B. Gan, Acta Mater. 55 (2007) 6561.
[28] H. Mosallaei, K. Sarabandi, IEEE Trans. Antennas Propag. 52 (2004) 1558.